A Space-Mapping Method for Object Location Estimation Adaptive to Camera Setup Changes for Vision-based Automation Applications†

Chih-Jen Wu and Wen-Hsiang Tsai

***Abstract*—A new space-mapping method for object location estimation, which is adaptive to camera setup changes, for use in various automation applications is proposed. The location of an object appearing in an image is estimated by mapping image coordinates of object points to corresponding real-world coordinates using a mapping table, which is constructed in two stages, with the first stage for establishing a basic table using bilinear interpolation in the camera manufacturing environment and the second for adapting the table to changes of camera heights and orientations in the application field. Analytic equations for table adaptation are derived by skillful utilization of both image formation and camera geometry properties. Good experimental results are shown to prove the feasibility of the proposed method.**

***Index Terms*—object location estimation, space mapping, table adaptation, camera setup changes.**

I. Introduction

Video cameras are used in various automation applications, including automatic estimations of object locations in indoor environments using object images acquired by cameras affixed to walls or ceilings. A conventional solution to the object location estimation problem is to conduct *camera calibration* to obtain a set of camera parameters, followed by using the parameters to compute the object location [1-6]. Most camera calibration methods use landmarks to compute camera parameters [4, 5], and the process is generally complicated. A flexible method based on this approach is proposed recently by Zhang [6], which only requires the camera to observe a planar pattern shown in a few different orientations. An alternative approach to object location estimation is to use a *space-mapping table* [7-10] which transforms the image space into the real-world space, thus avoiding the work of computing camera parameters. The table is constructed with the aid of a *calibration pattern* before the camera is deployed in an application environment.

† This work was supported financially by the Ministry of Economic Affairs under Project No. MOEA 97-EC-17-A-02-S1-032 in Technology Development Program for Academia.

C. J. Wu, Department of Computer Science, National Chiao Tung University, Hsinchu 30010, Taiwan; e-mail: gis91813@cis.nctu.edu.tw; Tel: +886-3-5131545; fax: +886-3-572-1490.

W. H. Tsai, Department of Computer Science, National Chiao Tung University, Hsinchu 30010, Taiwan; email: whtsai@asia.edu.tw; Tel: +886-3-5721489; fax: +886-3-572-1490; also with the Department of Information Communication, Asia University, Taichung 41354, Taiwan.

The space-mapping based approach to object location estimation, however, is *sensitive to camera setup changes*. That is, after a space-mapping table is constructed for a specific camera setup according to a certain *camera-environment configuration*, the camera should be used in *identical* configurations thereafter; otherwise, the table will not work. This weakness causes inconvenience in using the camera in various application fields.

To solve such a *camera-setup sensitive* problem for the space-mapping approach, one way is to construct a new table for every new camera-environment configuration. But this is often difficult to carry out after the camera is delivered to a user who does not know the mapping table construction process or/and has no calibration pattern for use in the field. In this study, we investigate the possibility of *automatically* modifying the original space-mapping table for use in the new environment. Note that this problem of adapting the space-mapping table to new camera setups has not been studied so far. The camera is assumed to be *general* in type with a *fixed* focal length and affixed to a ceiling. In case sharpness of taken images is concerned, a wide-angle camera with a small hyperfocal length of just a few inches may be used, which always takes sharp scene images at distances beyond a half of the hyperfocal length.

In the following, we first describe the idea and the detail of the proposed method in Sections II and III, respectively. Some experimental results are given in Section IV, followed by conclusions in Section V.

II. Idea of Proposed Method

The proposed method includes two stages, one conducted in an in-factory environment and the other in an in-field one. The details are described in the following algorithm. See Fig. 1 for an illustration.

Algorithm 1. Object location estimation by space-mapping table construction and modification.

Stage 1. Construction of a basic space-mapping table in the factory (see Fig. 1(a)).

Step. 1 Affix the camera to the ceiling at a certain height H_0 with the optical axis of the camera pointing to the floor perpendicularly.

Step. 2 Place a calibration pattern O on the ground right under the camera, take an image of it, extract relevant feature points from the image, and find the coordinates of them.

Step. 3 Measure the real-world coordinates of those feature

points in the calibration pattern which correspond to the extracted feature points in the image.

Step. 4 (*Coordinate mapping*) Use a quadrilateral mapping technique to construct a *basic space-mapping table* T, which maps each image coordinate pair (u_i, v_j) to a real-world coordinate pair (x_{ij}, y_{ij}).

Stage 2. Modifying the basic table for a new environment (see Fig 1(b)).

Step. 5 (*Ceiling-height adaptation*) If the new in-field camera setup to be carried out includes *just* a change of the original ceiling height H_0, perform the following operations to modify the basic table T; else, go to the next step.

5.1 Affix the camera to the ceiling and measure the new ceiling height H_1.

5.2 With H_1 as input, modify table T into a new one T_1 by a technique of *ceiling height adaptation* (described later in the next section), and go to Step 7.

Step. 6 (*Camera-orientation adaptation*) Perform the following operations to modify the basic table T.

6.1 Affix the camera to the ceiling, and measure the ceiling height L and the camera's orientation θ.

6.2 With L and θ as input, modify table T to be a new one T_1 by a technique of *camera orientation adaptation* (described later in the next section).

Step. 7 (*Location estimation*) Locate an object B in the real-world space using T_1 in the following way.

7.1 Acquired an image I of B with the camera.

7.2 Detect B in I and find a feature point p on it with coordinates (u, v).

7.3 Use (u, v) to look up T to get the real-world coordinates (x, y) of the real-world point P corresponding to p as the desired object location result.

Note that in the above algorithm, we assume that the processed object feature point in Step 7 is on the ground.

III. Basic Space-Mapping Table Construction and Modifications

As mentioned in Step 4 of Algorithm 1, a quadrilateral mapping technique has been designed in this study to perform the construction of a space-mapping table T by two steps: (1) finding pairs of corresponding quadrilaterals, one in the calibration pattern in the image and the other in the real world, and (2) transforming the image and real-world coordinates of corresponding points within the quadrilaterals using a bilinear interpolation technique, as illustrated by Figs. 2 and 3. The details are omitted due to the page limit.

After the basic table is obtained with the camera affixed to a ceiling at a certain height H_0 with respect to a floor F_0, if the camera is used later at a different ceiling height H_1 with respect to a second floor F_1, then the table is no more applicable and table content modification is necessary, which we call *ceiling-height adaptation*, as mentioned in Step 5 in Algorithm 1. To do this, first note that an image point p is formed in principle by *any* of the real-world points which all lie on a light ray R going into the camera's lens and then onto the image plane. As illustrated in Fig. 4(a), suppose that this light ray R intersects floor F_0 at P_0 and floor F_1 at P_1. If the image coordinates of p are (u, v), then the real-world coordinates (x_0, y_0) in the basic table corresponding to (u, v) actually are those of P_0 on F_0 instead of being the desired ones, (x_1, y_1), of P_1 on F_1. To correct this error, we derive first the following equalities according to the concept of *side proportionality* in a triangle:

$$x_1 = x_0 \frac{H_1}{H_0}; \qquad y_1 = y_0 \frac{H_1}{H_0}. \tag{1}$$

That is, the table lookup result (x_0, y_0) corresponding to the image coordinates (u, v) of a real-world point P_1 on F_1 should be magnified in proportion to H_1/H_0 to be (x_1, y_1) as the desired result. Note that we assume here: (1) the real-world coordinate system x-y-z is set up at the camera's lens center, (2) the optical axis is taken to be the z-axis, and (3) the location of object point P described by (x_1, y_1) is measured with respect to this system.

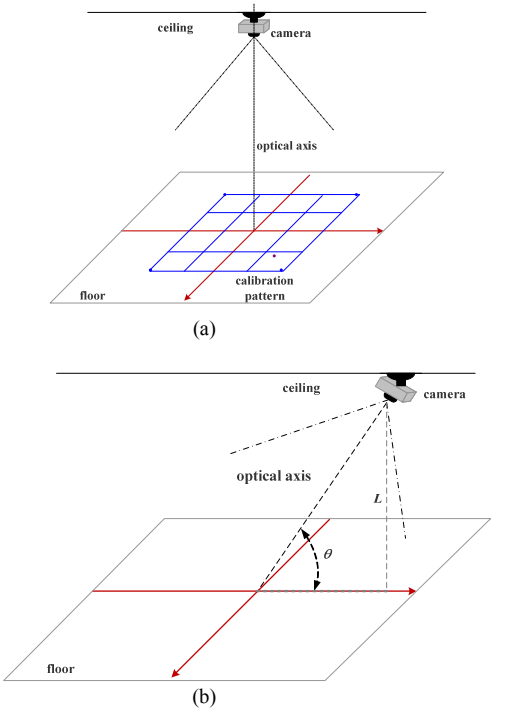

Fig. 1. Illustration of camera setup. (a) Construction of space-mapping table in Stage 1 of proposed method. (b) Camera setup changed to be with a new height of L and an additional tilt angle of θ.

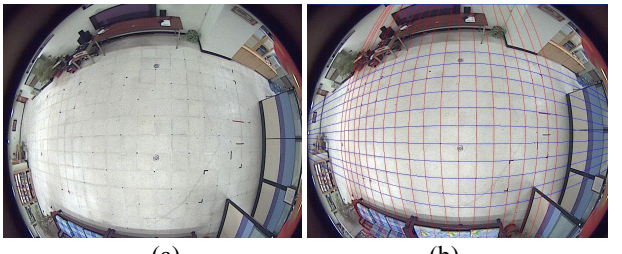

(a) (b)

Fig. 2. Illustration of quadrilateral shape extraction from a grid pattern on floor. (a) An image of the grid pattern. (b) The lines approximating the grid lines.

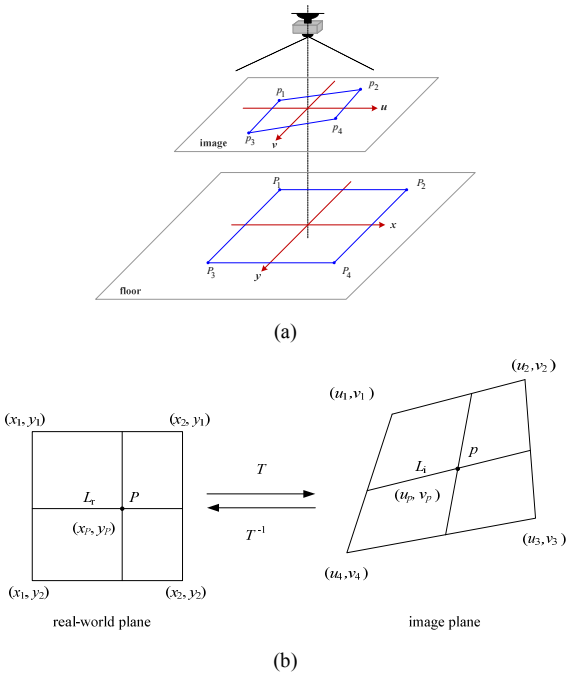

Fig. 3. Quadrilateral mapping. (a) Mapping of corresponding quadrilaterals in the image and the calibration pattern. (b) Location estimation of a space point by inverse bilinear interpolation.

Now, assume that the camera is affixed to the ceiling differently with a tilt angle of θ and a height of L with respect to floor F_1, as shown in Fig. 4(b). Here, the location of object point P_1 on F_1 to be estimated is specified by the real-world coordinates (x_1, y_1) with respect to the downward projection point O of the camera's lens center onto F_1, where the x-axis is assumed to be coincident with the projection of the camera's optical axis on F_1. Let the coordinates of P_1 in the acquired image be (u, v). Again the basic table is inapplicable here; the table lookup results, namely, the real-world coordinates (x_0, y_0), are actually those of a real-world point on a floor F_0 at a distance H_0 to the camera's lens center, instead of being the desired real-world coordinates (x_1, y_1) of P_1 on F_1. Again, table modification is necessary here, which is called *camera orientation adaptation* in Step 6 of Algorithm 1.

To correct the values (x_0, y_0) into (x_1, y_1), we rotate F_1 through an angle of $90^\circ - \theta$ with P_1 as the rotation pivot point, such that the resulting plane F_1' becomes perpendicular to the camera's optical axis and the lateral view of the rotation result seen from the positive y-axis direction becomes the one shown in Fig. 5. The original floor F_0 is also shown in the figure. Assume that the distance of P_1 on F_1' to the camera's optical axis is x'. Then, according to the concept of side proportionality again, we have

$$\frac{x_0}{x'} = \frac{H_0}{H_1}. \tag{2}$$

Also, by geometry and trigonometry we have

$$\sin\theta = \frac{x'}{M}; \tag{3}$$

$$\sin\theta = \frac{L}{N + H_0}; \tag{4}$$

$$\cos\theta = \frac{x_1 - M}{N + H_0}; \tag{5}$$

$$\cos\theta = \frac{H_1 - (N + H_0)}{M}. \tag{6}$$

From (4) and (5), we get $N + H_0 = L/\sin\theta = (x_1 - M)/\cos\theta$, or equivalently,

$$(x_1 - M)\sin\theta = L\cos\theta. \tag{7}$$

Also, from (2) and (3), we get $x_0/\sin\theta = MH_0/H_1$, or equivalently,

$$H_1 = \frac{H_0 M \sin\theta}{x_0}; \tag{8}$$

From (4), (6), and (8), we get

$$M = \frac{L}{\sin\theta} \times \frac{x_0}{H_0 \sin\theta - x_0 \cos\theta}. \tag{9}$$

And from (7) and (9), we get one of two desired coordinates:

$$x_1 = L \times \frac{H_0 \cos\theta + x_0 \sin\theta}{H_0 \sin\theta - x_0 \cos\theta}. \tag{10}$$

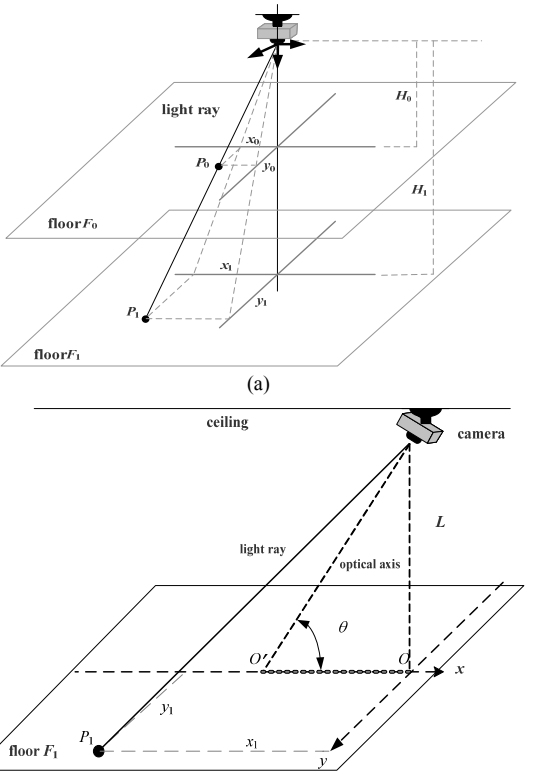

Fig. 4. Illustration of camera setup changes. (a) Use of side proportionality to compute coordinates of point P_1 on a floor F_1 with a ceiling height H_1. (b) A camera with tilt angle θ.

On the other hand, because the x-axis on F_1 is assumed to be coincident with the projection of the camera's optical axis on F_1

and because the rotation of F_1 into F_1' is pivoted in the y-direction, we have $y' = y_1$. Also, according to Eqs. (1) we have $y'/y_0 = H_1/H_0 = x'/x_0$. Therefore, $y_1 = y' = y_0(x'/x_0)$, from which and (3) and (9), we get the other desired coordinate:

$$y_1 = L \times \frac{y_0}{H_0 \sin\theta - x_0 \cos\theta} . \quad (11)$$

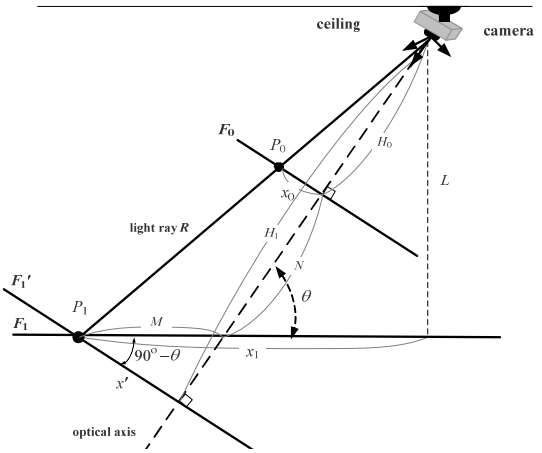

Fig. 5. Lateral view from positive y-axis direction of the rotation result of floor F_1 in Fig. 4(b) through an angle of $90^o - \theta$ with P_1 as the rotation pivot point.

IV. Experimental Results

A series of experiments using a fish-eye camera shown in Fig. 6(a) have been conducted to test the precision of the proposed method for object location estimation. The camera was attached to a rotator connected to a rod with an adjustable length, and so can be tilted arbitrarily and raised to any height. An image taken with the camera looking downward is shown in Fig. 2. We show additionally three images in Figs. 6(b) through 6(d) among those taken with the camera in two distinct categories of setups: (A) looking downward at the heights of 200cm, 225cm, and 250cm; (B) being tilted for 90^o, 70^o, and 50^o at the height of 200cm. The images are all of the resolution of 1280×1024.

The first case of Category-A setups at the height of 200cm was regarded as the *original* camera setup for building a basic space-mapping table. Specifically, after the image of Fig. 6(b) was taken with the downward-looking camera affixed at the height of 200cm, all the grid points in the image were extracted to get their image coordinates, forming a set I_c. Also, the real-world coordinates of each grid point were measured manually to form a set W_c. The two sets I_c and W_c were then used to construct a basic space-mapping table T.

To test the precision of Table T, nine non-grid points among the grid ones, which also appear in Fig. 6(b), were selected, and their image coordinates were collected to form a set I_c'. Also, the real-world coordinates of these non-grid points are measured manually to form another set W_c'. The set I_c' then was used to obtain their corresponding real-world coordinates by table lookup using T, forming a set denoted by W_c''. Finally, the two sets W_c' and W_c'' were compared and two types of error ratio measures were defined to compute the similarity between them:

(1) *type-1 location error ratio* ε_1 with respect to the distance from the real-world point to the camera's lens center:

$$\varepsilon_1 = \frac{\sqrt{(real\ x_i - estimated\ x_i)^2 + (real\ y_i - estimated\ y_i)^2}}{\sqrt{real\ x_i^2 + real\ y_i^2 + L^2}}$$

where *real* x_i and *real* y_i are data in W_c', and *estimated* x_i and *estimated* y_i are data in W_c'';

(2) *type-2 location error ratio* ε_2 with respect to the effective field of view of the camera:

$$\varepsilon_2 = \frac{\sqrt{(real\ x_i - estimated\ x_i)^2 + (real\ y_i - estimated\ y_i)^2}}{radius\ of\ effective\ camera's\ field\ of\ view} .$$

The computed results for the two types of error ratios are summarized in Table 1, from which we can see that the ratios are all smaller than 5% which are practical for object location estimation applications like indoor vehicle guidance.

Next, the cameras, still looking downward, were affixed at two different heights 225 and 250cm, and the corresponding error ratios were computed for some images taken by the camera (an example shown in Fig. 6(c)). The results were also summarized in Table 1, from which we can see the ratios are all smaller than 5% as well. Similarly, for Category-B setups where the cameras were affixed at the height 200cm and tilted for 90^o, 70^o, and 50^o, an error ratio table, namely, Table 3, was constructed as well for the images taken by the camera (an example shown in Fig. 6(d)). From the table, we can see that the ratios are *not* all smaller than 5% this time; instead, some are larger (6.4% and 7.5% in the last row in the table). A reason is that the object point dealt with is located at (–320, –15) which is far away from the image center, falls within a distorted-shaped quadrilateral, and so incurs a larger error in the quadrilateral mapping process. On the other hand, it can be seen from the two tables that the estimation accuracy decreases in general as the parameter value of the height, tilt angle, or object point distance increases.

Although the emphasis of this study is on adaptation of the space-mapping method to camera setup changes, we made additionally a comparison of the location estimation accuracy yielded by our method with those of two other methods [10, 11] whose accuracy results were reported in the literature. The comparison result is shown in Table 4, in which the average distance errors, the approximate vehicle movement range, and the average error percentage are shown. Some of the data were computed in this study from the available data in [10, 11]. From the table, we can see that the proposed method yields better object location accuracy than the other two methods.

V. Conclusions

A space-mapping method for object location estimation by modifying the basic space-mapping table for camera setup change adaptation has been proposed. The method does not require camera calibration, and is general for any camera type. The method estimates object locations by mapping the image coordinates of object points to the real-world ones using a space-mapping table. An algorithm is designed to construct the table in two stages: construction of a basic table using bilinear interpolation, and adaptation of the table to changes of camera

heights and orientations, which often occur in different application environments. Experimental results show that the method yields results with error ratios smaller than 5% in most cases, meaning the practicality of the method for various applications.

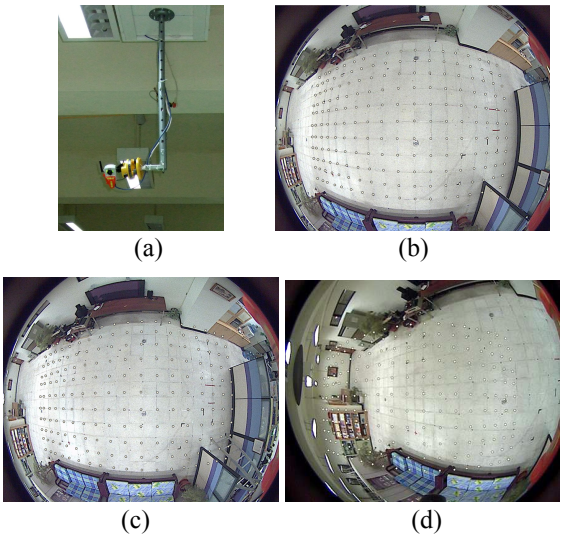

Fig. 6. Fish-eye camera and images used for experiments. (a) Camera setup. (b)-(d) Images taken respectively with the camera looking downward at heights 200cm and 250cm, and tilted for 50° at height 200cm.

ACKNOWLEDGEMENTS

A preliminary version of this paper appeared in *Knowledge-Based & Intelligent Information & Engineering Systems (Proc. KES 2009)*, *LNCS*, Vol. 5712, pp. 395-402, Sept. 2009.

REFERENCES

[1] Yang and W. H. Tsai, "Viewing corridors as right parallelepipeds for vision-based vehicle localization," *IEEE Trans. on Industrial Electronics*, Vol. 46, No. 3, pp. 653-661, June 1999.

[2] E. E. Hemayed, "A survey of camera self-calibration," *Proc. IEEE Conf. on Advanced Video & Signal Based Surveillance*, pp. 351- 357, Miami, Florida, USA, July 21-22, 2003.

[3] O. A. Aider, P. Hoppenot, and E. Colle, "A model-based method for indoor mobile robot localization using monocular vision and straight-line correspondences," *Robotics & Autonomous Systems*, Vol. 52, Issues 2-3, pp. 229-246, Aug. 2005.

[4] M. Betke and L. Gurvits, "Mobile robot localization using landmarks," *IEEE Trans. on Robotics & Automation*, Vol. 13, No. 2, pp. 251-263, April 1997.

[5] H. L. Chou and W. H. Tsai, "A new approach to robot location by house corners," *Pattern Recognition*, Vol. 19, No. 6, pp. 439-451, 1986.

[6] Z. Zhang, "A flexible new technique for camera calibration", *IEEE Trans. on Pattern Analysis & Machine Intelligence*, Vol. 22, No.11, pp. 1330-1334, 2000.

[7] H. C. Chen and W. H. Tsai, "Optimal security patrolling by multiple vision-based autonomous vehicles with omni-monitoring from the ceiling," *Proc. 2008 Int'l Computer Symp.,* Taipei, Taiwan, Nov. 13-15, 2008.

[8] S. W. Jeng and W. H. Tsai, "Using pano-mapping tables to unwarping of omni-images into panoramic and perspective-view Images," *IET Image Processing*, Vol. 1, No. 2, pp. 149-155, June 2007.

[9] Y. T. Wang and W. H. Tsai, "Indoor security patrolling with intruding person detection and following capabilities by vision-based autonomous vehicle navigation," *Proc. 2006 Int'l Computer Symposium (ICS 2006) - Workshop on Image Processing, Computer Graphics, & Multimedia Technologies*, Taipei, Taiwan, Dec. 4-6, 2006.

[10] T. Takeshita, T. Tomizawa and A. Ohya, "A house cleaning robot system – path indication and position estimation using ceiling camera," *Proc. Int'l Joint Conf. on SICE-ICASE*, pp. 2653-2656, Busan, Korea, Oct. 18-21, 2006.

[11] S. Y. Park, S. C. Jung, Y. S. Song and H. J. Kim, "Mobile robot localization in indoor environment using scale-invariant visual landmarks," *Proc. 2008 IAPR Workshop on Cognitive Information Processing*, pp. 159-163, Santorini, Greece, June 2008.

TABLE 1
ERROR RATIOS WITH CAMERA LOOKING DOWN AT DIFFERENT CEILING HEIGHT 200CM °, 225CM, AND 250CM.

real x,y (cm)	*real distance (cm)*	200cm		225cm		250cm	
		estimated (x, y) (cm)	*error ratios (type-1, type-2)*	*estimated (x, y) (cm)*	*error ratios (type-1, type-2)*	*estimated (x, y) (cm)*	*error ratios (type-1, type-2)*
(-7, -24)	25	(-8, -23)	(0.7%, 0.4%)	(-8, -24)	(0.5%, 0.3%)	(-9, -23)	(0.9%, 0.7%)
(-37, 36)	52	(-36, 36)	(0.5%, 0.3%)	(-37, 35)	(0.5%, 0.3%)	(-38, 37)	(0.6%, 0.4%)
(-20, 96)	98	(-20, 94)	(0.9%, 0.6%)	(-20, 95)	(0.4%, 0.3%)	(-21, 94)	(0.8%, 0.7%)
(-45, -107)	116	(-44, -106)	(0.6%, 0.4%)	(-46, -107)	(0.4%, 0.3%)	(-48, -109)	(1.3%, 1.1%)
(-111, -55)	124	(-112, -56)	(0.6%, 0.4%)	(-114, -56)	(1.3%, 1.0%)	(-117, -57)	(2.3%, 2.0%)
(-140, 62)	153	(-140, 60)	(0.8%, 0.6%)	(-143, 61)	(1.3%, 1.0%)	(-145, 62)	(1.7%, 1.6%)
(-229, -101)	250	(-228, -104)	(1.0%, 1.0%)	(-233, -106)	(2.0%, 2.0%)	(-238, -110)	(3.6%, 4.0%)
(-253, 76)	264	(-257, 82)	(2.2%, 2.3%)	(-260, 82)	(2.8%, 2.9%)	(-264, 80)	(3.2%, 3.7%)
(-320, -15)	320	(-317, -15)	(0.8%, 0.9%)	(-331, -14)	(2.9%, 3.4%)	(-335, -14)	(3.9%, 4.7%)
average error *ratio* (*type-1, type-2*)			(0.9%, 0.7%)		(1.4%, 1.3%)		(2.0%, 2.1%)

TABLE 2
ERROR RATIOS WITH CAMERA AT CEILING HEIGHT 200CM FOR DIFFERENT TILTED ANGLE 90°, 70°, AND 50°.

real x,y (cm)	*real distance (cm)*	Titled for 90°		Titled for 70°		Titled for 50°	
		estimated (x,y) (cm)	*error ratios (type-1, type-2)*	*estimated (x,y) (cm)*	*error ratios (type-1, type-2)*	*estimated (x,y) (cm)*	*error ratios (type-1, type-2)*
(-7, -24)	25	(-8, -23)	(0.7%, 0.4%)	(-7, -22)	(1.0%, 0.6%)	(-7, -22)	(1.0%, 0.6%)
(-37, 36)	52	(-36, 36)	(0.5%, 0.3%)	(-37, 52)	(1.5%, 0.9%)	(-38, 34)	(1.1%, 0.7%)
(-20, 96)	98	(-20, 94)	(0.9%, 0.6%)	(-22, 94)	(1.3%, 0.9%)	(-21, 90)	(2.7%, 1.9%)
(-45, -107)	116	(-44, -106)	(0.6%, 0.4%)	(-45, 103)	(1.7%, 1.2%)	(-42, -103)	(2.2%, 1.6%)
(-111, -55)	124	(-112, -56)	(0.6%, 0.4%)	(-115, -58)	(2.1%, 1.6%)	(-110, -60)	(2.2%, 1.6%)
(-140, 62)	153	(-140, 60)	(0.8%, 0.6%)	(-144, 66)	(2.2%, 1.8%)	(-141, 58)	(1.6%, 1.3%)
(-229, -101)	250	(-228, -104)	(1.0%, 1.0%)	(-224, -95)	(2.4%, 2.4%)	(-238, -110)	(4.0%, 4.0%)
(-253, 76)	264	(-257, 82)	(2.2%, 2.3%)	(-259, 82)	(2.6%, 2.6%)	(-271, 81)	(4.5%, 4.6%)
(-320, -15)	320	(-317, -15)	(0.8%, 0.9%)	(-330, -16)	(2.7%, 3.1%)	(-340, -26)	(6.0%, 7.1%)
average error *ratio* (*type-1, type-2*)			(0.9%, 0.7%)		(1.9%, 1.7%)		(2.8%, 2.6%)

TABLE 3
COMPARASION OF VEHICLE LOCALIZATION ACCURACY

	Takeshita et al	*Park et al.*	*Our Method*
Average distance error	4.6cm	26cm	5.8cm
Approximate range of vehicle movement	2.1m	7m	6.4m
Average error percentage	5.6%	3.7%	0.9%